A Control-Oriented Modeling Approach to Spatial Neutronics Simulation of a Lead-Cooled Fast Reactor

S. Lorenzi
Politecnico di Milano,
Department of Energy,
via la Masa 34, 20156 Milano, Italy
e-mail: stefano.lorenzi@polimi.it

A. Cammi
Politecnico di Milano,
Department of Energy,
via la Masa 34, 20156 Milano, Italy
e-mail: antonio.cammi@polimi.it

L. Luzzi[1]
Politecnico di Milano,
Department of Energy,
via la Masa 34, 20156, Milano, Italy
e-mail: lelio.luzzi@polimi.it

R. Ponciroli
Politecnico di Milano,
Department of Energy,
via la Masa 34, 20156 Milano, Italy
e-mail: roberto.ponciroli@polimi.it

1 Introduction

The need for improving plant availability and the present energy production situation require constantly enhanced performance for nuclear power plants (NPPs), along with an increasing ability to follow grid demands [1]. In this context, the control of nuclear reactor plays a fundamental role in order to improve the plant-operational flexibility. This can be obtained by employing innovative control techniques made available due to the significant developments of digital instrumentation & control (I&C) technology in last decades. On the other hand, these techniques require a more accurate modeling approach, which may provide more detailed information regarding neutron flux, temperature, pressure, and mass flow rate used for diagnostics and fault detection during operational transients [2]. The latter aspect is of particular interest for innovative reactor concepts; for instance, Generation IV reactors [3] are characterized by power density and temperature ranges (experienced by structural materials) such that the corresponding spatial dependence cannot be neglected.

In the light of the previous considerations, it is of primary importance to rely on simulation tools devoted to the control system development for both its realization and validation by means of an accurate description of the reactor-controlled response. Different from a system code or dynamic tools for safety study, a simulation tool for control purposes has to fulfill some typical requirements. In particular, fast-running simulations, a comprehensive representation of the entire plant behavior, and the possibility to couple the plant dynamics simulator with the control system model are the main requests. In order to accomplish these goals, among the several modeling options, the object-oriented modeling constitutes a suitable choice for the model-based control design due to the features of this approach (i.e., the hierarchical structure, the abstraction, and the encapsulation), which allow developing a model that satisfies the requirements of modularity, openness, and efficiency [4]. A viable path to achieve the aforementioned objectives is by adoption of the Modelica language [5]. Introduced in 1997, Modelica is an object-oriented modeling language specifically designed for the study of engineering system dynamics in the control field [6]. Modelica is declarative, as it focuses on what the model should describe, leaving the numerical issues entirely to the compiler. Modelica is equation-based as it facilitates the system description in terms of physical/engineering principles (i.e., mass, energy, and momentum balance equations), implementing sets of differential algebraic and discrete equations. These features allow acausal modeling (i.e., the direct use of equations without imposing the classic input/output declaration), granting a more flexible and efficient data flow [6]. Finally, Modelica favors the physical modeling (i.e., the model components correspond to plant components); it is open source and has already been successfully adopted in different fields, such as automotive, robotics, thermohydraulic, and mechatronic systems, and as well as the nuclear simulation field [7–9].

As far as the reactor neutronics description is concerned, point kinetics (PK) [10] is commonly employed in control-oriented tools. This lumped parameter approach describes the time dependence of the neutron population in the reactor and relates it to the flux by a constant of proportionality (single-energy group approximation). The approach neglects the spatial dependence of the variables, such

[1]Corresponding author.
Manuscript received October 14, 2014; final manuscript received January 28, 2015; published online May 20, 2015.

an assumption being valid if the system reaches the critical state and if there are no large localized perturbations [11]. The system reactivity feedback is usually expressed as a linear function of the mean values of characteristic temperatures with constant coefficients. The resulting model is represented by a set of ordinary differential equations (ODEs), which are suitable for control purposes as they usually fulfill the mentioned requirements, and they can be easily linearized in order to study the system with linear analysis tools. Notwithstanding, the adoption of such simplified description precludes the possibility of exploiting all the capabilities of advanced control schemes, limiting the achievable control performance. On the other hand, the solution of the time-dependent partial differential equation (PDE) related to the neutron diffusion cannot be directly exploited for control system studies. Indeed, besides the high computational burden, it does not allow immediately to get the system-governing dynamics without a proper postprocessing.

It is thus necessary to develop a sufficiently accurate description of the reactor core spatial dynamics, preferably based on a set of ODEs. One option is to use the modal method (MM) [12], which has been proven to give better results than a multipoint kinetics approach [13]. The MM was theorized in the 1960s, but it was not systematically employed for dynamics simulations because of the high computational burden for the determination of the higher order eigenfunctions. This method allows separating the spatial and time dependence of the neutron flux, which can be represented as the sum of the eigenfunctions of the neutron diffusion PDE weighted by time-dependent coefficients. The eigenfunction calculation is performed only once as an *offline* phase of the entire procedure. The dynamic behavior of the flux is reduced to the study of these time-dependent coefficients and can be represented by a set of ODEs. Even if the MM has already been proposed for control purposes [14,15], the feasibility of its implementation in a control-oriented simulator has never been systematically studied. In particular, a generalized multigroup energy modeling necessary for studying fast reactor systems, with the direct incorporation of the reactivity thermal feedbacks, has never been assessed, along with the coupling with a heat transfer model. In the present work, in order to test the capabilities of this method for reproducing the reactivity, the neutron flux shape, and the characteristic temperatures at different reactor conditions, the lead-cooled fast reactor (LFR) has been considered. Indeed, in this reactor concept, the thermal power density and the temperature field assume a particular importance because of the corrosion phenomena due to the use of a chemically aggressive coolant as lead. Therefore, it is fundamental to evaluate the distribution of reactivity thermal feedbacks accurately, so as to verify that during the operational transients the technological constraints are respected in any part of the system.

The paper is organized as follows. In Section 2, after a brief introduction of the LFR system employed as a case study, the MM employed for the spatial neutronics simulation is presented with the description of the several phases involved in the procedure. Section 3 describes the simulation tool developed for the test case, with a specific focus on the modal neutronics (MN) and heat transfer components of the object-oriented model. Finally, the simulation results are presented in order to test the MM capabilities (Section 4), and the main conclusions are outlined in Section 5.

2 Modal Method

2.1 System Description. The Advanced Lead Fast-Reactor European Demonstrator (ALFRED) developed within the European FP7 LEADER (Lead-cooled European Advanced Demonstration Reactor) Project has been employed as a case study [16]. In particular, a test case involving three fuel pins has been set up and investigated (Fig. 1). The main fuel pin data are reported in Table 1 [17].

2.2 Procedure Description. In order to describe the neutron kinetics, the multigroup diffusion theory [18], with six energy groups and eight groups of precursors, has been considered, and can be written as

$$\underline{\underline{V}}^{-1}\frac{\partial \underline{\phi}}{\partial t} = \nabla\cdot(\underline{\underline{D}}\nabla\underline{\phi}) - \underline{\underline{\Sigma}}_a\underline{\phi} - \underline{\underline{\Sigma}}_s\underline{\phi} + (1-\beta)\underline{\chi}_p\underline{F}^T\underline{\phi} + \sum_j \lambda_j\underline{\chi}_d C_j \tag{1}$$

$$\frac{\partial C_j}{\partial t} = -\lambda_j C_j + \beta_j \underline{F}^T\underline{\phi}, \qquad j = 1 \div 8 \tag{2}$$

where

$$\underline{\phi}(\mathbf{r},t) = \begin{bmatrix}\phi_1(\mathbf{r},t)\\ \vdots \\ \phi_6(\mathbf{r},t)\end{bmatrix} \qquad \phi_g(\mathbf{r},t) = \int_{E_g}^{E_{g-1}} \mathrm{d}E\phi(\mathbf{r},E,t) \quad g = 1 \div 6$$

$$\underline{\underline{V}}^{-1} = \mathrm{diag}\left(\frac{1}{v_g}(\mathbf{r})\right) \qquad \underline{\underline{D}} = \mathrm{diag}(D_g(\mathbf{r})) \qquad \underline{\underline{\Sigma}}_a = \mathrm{diag}(\Sigma_a^g(\mathbf{r}))$$

$$\underline{\underline{\Sigma}}_s = \begin{bmatrix} \Sigma_s^{1\to}(\mathbf{r}) & -\Sigma_s^{2\to1}(\mathbf{r}) & \cdots & -\Sigma_s^{6\to1}(\mathbf{r}) \\ -\Sigma_s^{1\to2}(\mathbf{r}) & \Sigma_s^{2\to}(\mathbf{r}) & \cdots & -\Sigma_s^{6\to2}(\mathbf{r}) \\ \vdots & \vdots & \ddots & \vdots \\ -\Sigma_s^{1\to6}(\mathbf{r}) & -\Sigma_s^{2\to6}(\mathbf{r}) & \cdots & \Sigma_s^{6\to}(\mathbf{r}) \end{bmatrix}$$

$$\underline{\chi}_p = \begin{bmatrix}\chi_p^1\\ \vdots \\ \chi_p^6\end{bmatrix} \qquad \underline{\chi}_d = \begin{bmatrix}\chi_d^1\\ \vdots \\ \chi_d^6\end{bmatrix} \qquad \underline{F}^T = [\,\nu\Sigma_f^1(\mathbf{r}) \quad \cdots \quad \nu\Sigma_f^6(\mathbf{r})\,] \tag{3}$$

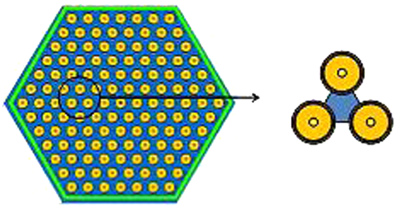

Fig. 1 ALFRED subchannel adopted as a case study

Table 1 ALFRED fuel pin parameters

Fuel pin design parameter	Value
Average pin power, kW	≈13.7
Coolant inlet temperature, °C	400
Average coolant outlet temperature, °C	480
Average coolant velocity, m s^{-1}	≈1.4
Fuel type	MOX
Average enrichment as Pu/(Pu + U), wt%	25.77
Cladding	Ti-15-15
Fill gas	He
Active length, mm	600
Cladding outer diameter, mm	10.5
Cladding inner diameter, mm	9.3
Fuel pellet outer diameter, mm	9
Fuel pellet inner diameter, mm	2
Pin pitch, mm	13.86

The MM allows describing the neutron flux as[1]

$$\underline{\phi}(\mathbf{r},t) \cong \sum_{i=1}^{N} \underline{\underline{\psi}}_i(\mathbf{r}) \cdot \underline{n}_i(t) \tag{4}$$

where $\underline{\underline{\Psi}}_i(\mathbf{r})$ is a spatial basis where the flux is projected and $\underline{n}_i(t)$ are the time-dependent coefficients, which are the unknowns of the obtained ODEs system

$$\underline{\underline{\psi}}_i(\mathbf{r}) = \begin{bmatrix} \psi_i^1(\mathbf{r}) & 0 & 0 \\ 0 & \ddots & 0 \\ 0 & 0 & \psi_i^6(\mathbf{r}) \end{bmatrix} = \mathrm{diag}(\underline{\psi}_i(\mathbf{r})) \tag{5}$$

$$\underline{n}_i(t) = \begin{bmatrix} n_i^1(t) \\ \vdots \\ n_i^6(t) \end{bmatrix} \tag{6}$$

In the MM, the basis functions are the eigenfunctions associated with the neutron diffusion equation, calculated in a reference configuration. The eigenvalue problem is

$$(-\nabla \cdot \underline{\underline{D}}\nabla + \underline{\underline{\Sigma}}_a + \underline{\underline{\Sigma}}_s)\underline{\psi}_i = \lambda_i^* \underline{\chi}_p \underline{F}^T \underline{\psi}_i \tag{7}$$

where the first eigenfunction $\underline{\Psi}_1$ gives the fundamental flux distribution. The core criticality condition is determined by the inverse of the first eigenvalue, λ_1^*. The former equation can be rewritten in the operator theory fashion as follows

$$L\underline{\psi}_i = \lambda_i^* M \underline{\psi}_i \quad L = -\nabla \cdot (\underline{\underline{D}}\nabla) + \underline{\underline{\Sigma}}_a + \underline{\underline{\Sigma}}_s \quad M = \underline{\chi}_p \underline{F}^T \tag{8}$$

where L and M operators are the neutronics removal operator and the production operator, respectively.

In order to transform the multigroup diffusion PDEs into a set of ODEs involving only the time-dependent coefficient $\underline{n}_i(t)$, the expression of Eq. (4) has to be substituted into Eqs. (1) and (2), the latter have to be multiplied by test functions and integrated over the computational domain. As suitable test functions, the eigenfunctions of the adjoint generalized problem associated to Eq. (8), $\underline{\underline{\Psi}}_i^\dagger$, have been employed as they are related to the neutron importance. This procedure can be related to a Petrov–Galerkin projection.

The offline procedure to obtain the set of ODEs is the following:

1. compute N eigenfunctions $\underline{\Psi}_i$ from Eq. (8)
2. compute N adjoint eigenfunctions $\underline{\Psi}_i^\dagger$ from the adjoint problem
3. substitute the expression of Eq. (4) into Eqs. (1) and (2)
4. premultiply Eq. (1) by $\underline{\underline{\Psi}}_i^\dagger$ and Eq. (2) by $\underline{\underline{\Psi}}_i^\dagger \underline{\chi}_d$
5. integrate over the spatial domain Ω

The number of the adopted eigenfunctions has an impact on the accuracy of the representation. In general, the higher the number of the eigenfunctions, the better the dynamic behavior is represented in case of strong perturbation of the system. On the other hand, a large number of eigenfunctions entails more computational effort both in the offline calculation and in the ODE system simulation.

The calculation of eigenfunctions and adjoint eigenfunctions of the neutron diffusion equation with six energy groups has been performed through the finite element COMSOL Multiphysics software [20] (Fig. 2(*a*)). The mesh employed (Fig. 2(*b*)) features a 3D geometry using Lagrangian and linear-order triangular prism and hexahedral elements. In this way, a good compromise between numerical accuracy and computational requirements has been achieved, confirmed by a mesh sensitivity test as well. The neutronic parameters $(\underline{\underline{V}}^{-1}, \underline{\underline{D}}, \underline{\underline{\Sigma}}_a, \underline{\underline{\Sigma}}_s, \underline{\chi}_p, \underline{F}^T, \underline{\chi}_d)$ of the six energy groups (Table 2) have been assessed by means of the continuous energy Monte Carlo neutron transport code SERPENT [21] featuring its group constant-generation capabilities. Simulations have been carried out at different fuel and lead temperatures to derive the trend of the temperature- and density-dependent cross sections and diffusion coefficients. In the fuel, the dependency of the macroscopic neutron cross sections on the local temperature and density has been taken into account, whereas for lead cross sections, the Doppler broadening effect has been neglected [22], obtaining the following equations

$$\Sigma_f(T,d) = \left(\frac{d}{d_0}\right)\left[\Sigma_{f,0} + A \cdot \log\left(\frac{T}{T_0}\right)\right] \tag{9}$$

$$\Sigma_l(d) = \left(\frac{d}{d_0}\right)\Sigma_{l,0} \tag{10}$$

The other neutronics parameters, which are calculated at nominal conditions, are kept constant during the simulations. As far as the boundary conditions are concerned, the albedo boundary conditions are imposed at the axial and radial boundaries of the COMSOL model domain, namely

$$n \cdot (D_g \nabla \phi_g) = \gamma_a \phi_g \qquad n \cdot (D_g \nabla \phi_g) = \gamma_r \phi_g \tag{11}$$

A "reference model" implementing the multigroup diffusion equations, Eqs. (1) and (2), has been developed in COMSOL and coupled with a heat transfer model in order to obtain a reference solution for the assessment of the MM results both in static and

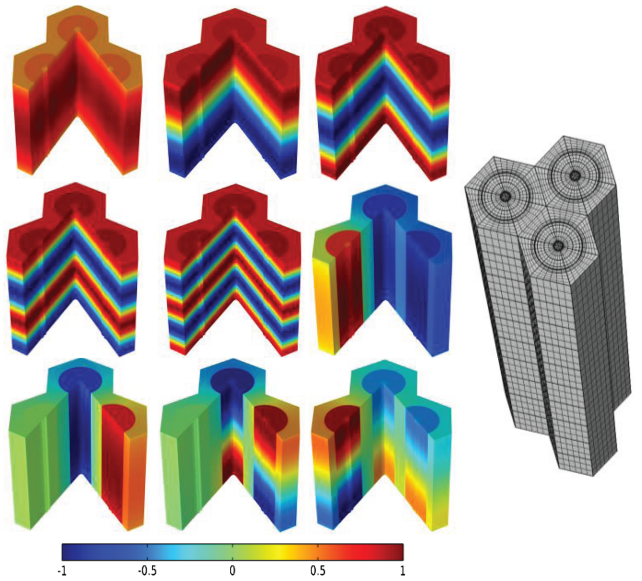

Fig. 2 (*a*) First nine neutronics spatial modes (normalized flux); (*b*) computational mesh

Table 2 Energy group boundaries adopted in multigroup diffusion equations

Group	Upper boundary	Lower boundary
1	20 MeV	2.23 MeV
2	2.23 MeV	0.82 MeV
3	0.82 MeV	67.38 keV
4	67.38 keV	15.03 keV
5	15.03 keV	0.75 keV
6	0.75 keV	0 keV

[1]Although the completeness of the eigenfunctions set is not proved, it is the current practice to assume it [19].

dynamic conditions. The reader may refer to Ref. [23] for additional information on the neutronic input generation, the calculation of the eigenfunctions, and the "reference model."

After the Galerkin projection, the ODE system for the time-dependent coefficients can be expressed, for each eigenfunction, as

$$\sum_{m=1}^{N} \underline{\underline{RV}}_{im} \cdot \dot{\underline{n}}_m = \sum_{m=1}^{N} \left(-\underline{\underline{L}}_{im} - \underline{\underline{\delta L}}_{im} + (1-\beta) \cdot (\underline{\underline{M}}_{im} + \underline{\underline{\delta M}}_{im}) \right) \cdot \underline{n}_m + \sum_{j=1}^{8} \lambda_j \underline{c}_{ij} \tag{12}$$

$$\dot{\underline{c}}_{ij} = \beta_j \underline{\underline{X}} \left[\sum_{m=1}^{N} (\underline{\underline{M}}_{im} + \underline{\underline{\delta M}}_{im}) \cdot \underline{n}_m \right] - \lambda_j \underline{c}_{ij}, \quad j = 1 \div 8 \tag{13}$$

with the following initial conditions

$$\begin{aligned} \underline{n}_1 &= (1 \ \cdots \ 1)^T \quad \underline{n}_{i\neq 1} = (0 \ \cdots \ 0)^T \\ \underline{c}_{1,j} &= \tfrac{\beta_j}{\lambda_j} \underline{\underline{X}} \cdot \underline{\underline{M}}_{11} \cdot \underline{n}_1 \qquad \underline{c}_{i\neq 1,j} = (0 \ \cdots \ 0)^T \end{aligned} \tag{14}$$

where

$$\underline{\underline{RV}}_{im} = \int \underline{\psi}_i^{\dagger} \cdot \underline{\underline{V}}^{-1} \cdot \underline{\psi}_m \, \mathrm{d}\Omega \qquad \underline{\underline{L}}_{im} = \int \underline{\psi}_i^{\dagger} \cdot L \underline{\psi}_m \, \mathrm{d}\Omega$$

$$\underline{\underline{\delta L}}_{im} = \int \underline{\psi}_i^{\dagger} \cdot \delta L \underline{\psi}_m \, \mathrm{d}\Omega \qquad \underline{\underline{M}}_{im} = \int \underline{\psi}_i^{\dagger} \cdot M \underline{\psi}_m \, \mathrm{d}\Omega$$

$$\underline{\underline{\delta M}}_{im} = \int \underline{\psi}_i^{\dagger} \cdot \delta M \underline{\psi}_m \, \mathrm{d}\Omega \qquad \underline{c}_{ij} = \int \underline{\psi}_i^{\dagger} \cdot \underline{\chi}_d \cdot C_j \mathrm{d}\Omega$$

$$\underline{\underline{X}} = \begin{bmatrix} \chi_d^1/\chi_p^1 & 0 & 0 \\ 0 & \ddots & 0 \\ 0 & 0 & \chi_d^6/\chi_p^6 \end{bmatrix} \tag{15}$$

$\underline{\underline{L}}_{im}$ and $\underline{\underline{M}}_{im}$ represent the contribution of the ith eigenfunction to the removal and production operator calculated in the unperturbed system (i.e., the configuration on which the eigenfunctions are calculated). These quantities are calculated once in the "offline" process and are kept constant during the transient simulation. On the other hand, $\underline{\underline{\delta L}}_{im}$ and $\underline{\underline{\delta M}}_{im}$ represent the variation of the removal and the production operators during the transients, for instance, due to the density and temperature change of the cross sections. Such effects constitute the reactivity feedbacks, which assume a particular relevance in the control-oriented perspective. According to this procedure, the variation is weighted on the spatial basis functions, which allow accounting the spatial characteristics of

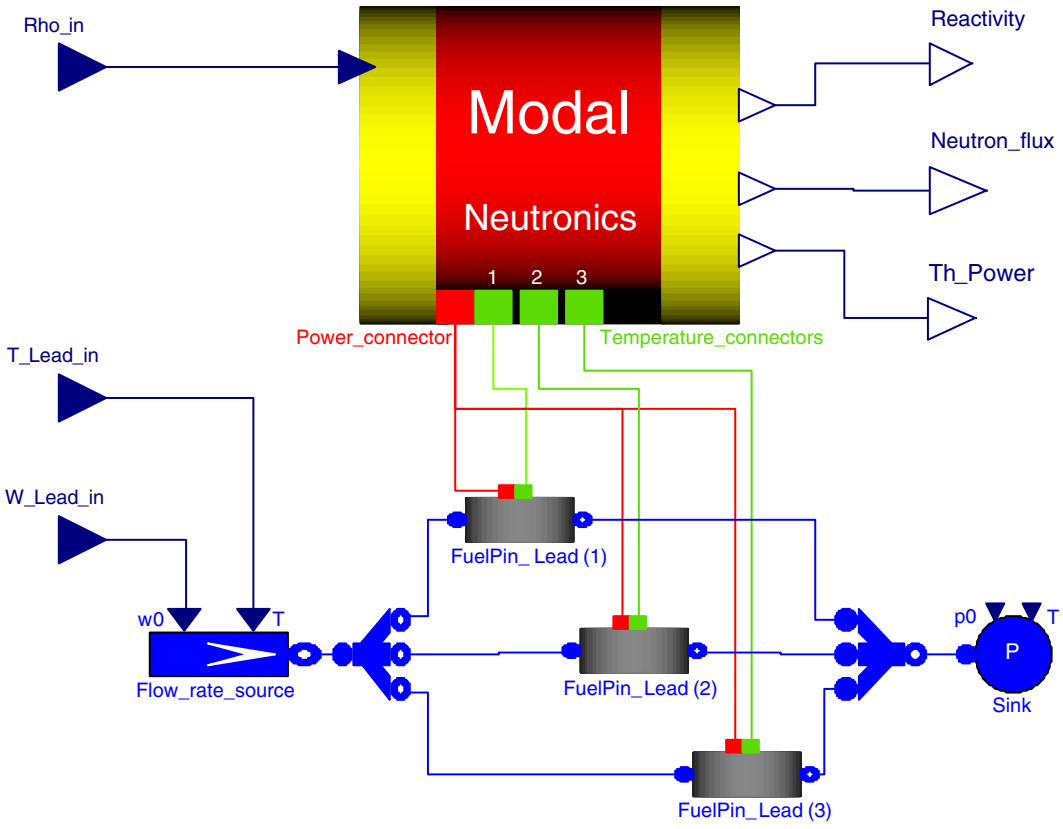

Input variables	Definition
T__Lead_in	Lead inlet temperature
W_Lead_in	Lead mass flow rate
Rho_in	External reactivity
Output variables	**Definition**
Reactivity	Total reactivity system
Neutron_flux	Neutron flux
Th_Power	Thermal power

Fig. 3 Object-oriented model of the test case

the perturbation and obtaining an accurate estimation of the reactivity evolution. This goal cannot be achieved with a PK approach as the reactivity variations are uniformly evaluated through the system.

3 Object-Oriented Model

The control-oriented tool of the ALFRED test case has been developed adopting the object-oriented modeling, based on the Modelica language. The overall model (Fig. 3) has been built by connecting different components (i.e., objects described by equations), through rigorously defined interfaces (connectors) corresponding to the physical interactions occurring with the external environment or other objects. Dymola (Dynamic Modeling Laboratory) [24] has been adopted as simulation environment because dedicated libraries of validated models for power plant components are available. In particular, the two main components are the *MN* and the *FuelPin_Lead*, the latter being the component describing the heat transfer inside a fuel pin and the surrounding lead. In the following sections, the components specifically modeled in this paper (i.e., the MN and heat transfer of the fuel pin) will be described in detail, whereas for the most conventional ones (i.e., the mass flow rate source, and the sink), the *ThermoPower* library has been employed [25].

3.1 Modal Neutronics Component. The MN component employs a kinetics model based on the MM described in Section 2. In particular, the set of Eqs. (12) and (13) has been expressed in a general and compact matrix format as

$$\dot{\underline{n}} = \underline{\underline{iRV}} \cdot [(\underline{\underline{A}}_{1,np} + \underline{\underline{A}}_{1,p})\underline{n} + \underline{\underline{A}}_2 \underline{c}] \tag{16}$$

$$\dot{\underline{c}} = (\underline{\underline{A}}_{3,np} + \underline{\underline{A}}_{3,p})\underline{n} - \underline{\underline{A}}_4 \underline{c} \tag{17}$$

where

$$\underline{n} = [\underline{n}_1; \underline{n}_2; \ldots; \underline{n}_N]^T \quad \underline{c} = [\underline{c}_{11}; \underline{c}_{12}; \ldots; \underline{c}_{1P}; \underline{c}_{21}; \ldots; \underline{c}_{NP}]^T \quad \underline{\underline{iRV}} = \begin{bmatrix} \underline{\underline{RV}}_{11} & \cdots & \underline{\underline{RV}}_{1N} \\ \vdots & \ddots & \vdots \\ \underline{\underline{RV}}_{N1} & \cdots & \underline{\underline{RV}}_{NN} \end{bmatrix}^{-1}$$

$$\underline{\underline{A}}_{1,np} = \begin{bmatrix} -\underline{\underline{L}}_{11} + (1-\beta)\underline{\underline{M}}_{11} & \cdots & -\underline{\underline{L}}_{1N} + (1-\beta)\underline{\underline{M}}_{1N} \\ \vdots & \ddots & \vdots \\ -\underline{\underline{L}}_{N1} + (1-\beta)\underline{\underline{M}}_{N1} & \cdots & -\underline{\underline{L}}_{NN} + (1-\beta)\underline{\underline{M}}_{NN} \end{bmatrix} \quad \underline{\underline{A}}_{1,p} = \begin{bmatrix} -\underline{\underline{\delta L}}_{11} + (1-\beta)\underline{\underline{\delta M}}_{11} & \cdots & -\underline{\underline{\delta L}}_{1N} + (1-\beta)\underline{\underline{\delta M}}_{1N} \\ \vdots & \ddots & \vdots \\ -\underline{\underline{\delta L}}_{N1} + (1-\beta)\underline{\underline{\delta M}}_{N1} & \cdots & -\underline{\underline{\delta L}}_{NN} + (1-\beta)\underline{\underline{\delta M}}_{NN} \end{bmatrix}$$

$$\underline{\underline{\lambda}}_j = \lambda_j \underline{\underline{I}} \quad j = 1 \div 8 \qquad \underline{\underline{A}}_2 = \begin{bmatrix} \underline{\underline{\lambda}}_1 & \cdots & \underline{\underline{\lambda}}_p & \underline{\underline{0}} & \underline{\underline{0}} & \underline{\underline{0}} & \underline{\underline{0}} \\ \underline{\underline{0}} & \underline{\underline{0}} & \underline{\underline{0}} & \ddots & \underline{\underline{0}} & \underline{\underline{0}} & \underline{\underline{0}} \\ \underline{\underline{0}} & \underline{\underline{0}} & \underline{\underline{0}} & \underline{\underline{0}} & \underline{\underline{\lambda}}_1 & \cdots & \underline{\underline{\lambda}}_p \end{bmatrix} \quad \underline{\underline{A}}_{3,np} = \begin{bmatrix} \beta_1 \underline{\underline{X}} \cdot \underline{\underline{M}}_{11} & \cdots & \beta_1 \underline{\underline{X}} \cdot \underline{\underline{M}}_{1N} \\ \vdots & \cdots & \vdots \\ \beta_P \underline{\underline{X}} \cdot \underline{\underline{M}}_{11} & \cdots & \beta_P \underline{\underline{X}} \cdot \underline{\underline{M}}_{1N} \\ \vdots & \ddots & \vdots \\ \beta_1 \underline{\underline{X}} \cdot \underline{\underline{M}}_{N1} & \cdots & \beta_1 \underline{\underline{X}} \cdot \underline{\underline{M}}_{NN} \\ \vdots & \cdots & \vdots \\ \beta_P \underline{\underline{X}} \cdot \underline{\underline{M}}_{N1} & \cdots & \beta_P \underline{\underline{X}} \cdot \underline{\underline{M}}_{NN} \end{bmatrix} \tag{18}$$

$$\underline{\underline{A}}_{3,p} = \begin{bmatrix} \beta_1 \underline{\underline{X}} \cdot \underline{\underline{\delta M}}_{11} & \cdots & \beta_1 \underline{\underline{X}} \cdot \underline{\underline{\delta M}}_{1N} \\ \vdots & \cdots & \vdots \\ \beta_P \underline{\underline{X}} \cdot \underline{\underline{\delta M}}_{11} & \cdots & \beta_P \underline{\underline{X}} \cdot \underline{\underline{\delta M}}_{1N} \\ \vdots & \ddots & \vdots \\ \beta_1 \underline{\underline{X}} \cdot \underline{\underline{\delta M}}_{N1} & \cdots & \beta_1 \underline{\underline{X}} \cdot \underline{\underline{\delta M}}_{NN} \\ \vdots & \cdots & \vdots \\ \beta_P \underline{\underline{X}} \cdot \underline{\underline{\delta M}}_{N1} & \cdots & \beta_P \underline{\underline{X}} \cdot \underline{\underline{\delta M}}_{NN} \end{bmatrix} \quad \underline{\underline{A}}_4 = \begin{bmatrix} \underline{\underline{\lambda}}_1 & \underline{\underline{0}} & \underline{\underline{0}} & \underline{\underline{0}} & \underline{\underline{0}} & \underline{\underline{0}} & \underline{\underline{0}} \\ \underline{\underline{0}} & \ddots & \underline{\underline{0}} & \underline{\underline{0}} & \underline{\underline{0}} & \underline{\underline{0}} & \underline{\underline{0}} \\ \underline{\underline{0}} & \underline{\underline{0}} & \underline{\underline{\lambda}}_P & \underline{\underline{0}} & \underline{\underline{0}} & \underline{\underline{0}} & \underline{\underline{0}} \\ \underline{\underline{0}} & \underline{\underline{0}} & \underline{\underline{0}} & \ddots & \underline{\underline{0}} & \underline{\underline{0}} & \underline{\underline{0}} \\ \underline{\underline{0}} & \underline{\underline{0}} & \underline{\underline{0}} & \underline{\underline{0}} & \underline{\underline{\lambda}}_1 & \underline{\underline{0}} & \underline{\underline{0}} \\ \underline{\underline{0}} & \underline{\underline{0}} & \underline{\underline{0}} & \underline{\underline{0}} & \underline{\underline{0}} & \ddots & \underline{\underline{0}} \\ \underline{\underline{0}} & \underline{\underline{0}} & \underline{\underline{0}} & \underline{\underline{0}} & \underline{\underline{0}} & \underline{\underline{0}} & \underline{\underline{\lambda}}_P \end{bmatrix}$$

According to the purposes of this work, the variation of removal and production operators is due to temperature and density change of material (i.e., the reactivity thermal feedbacks of fuel and lead). The temperatures are calculated in the component *FuelPin_Lead* and the information shared with the *MN* component by means of connectors (see Fig. 3).

For the neutronics calculation, the geometry has been divided into four radial coarse zones (three for the fuel, inner, central, and outer, and one for the lead) and into 10 evenly spaced axial zones. For each region, the reactivity insertion is weighted on the spatial basis functions integrated over the zone (not over all the system as it happens for $\underline{\underline{L}}_{im}$ and $\underline{\underline{M}}_{im}$), considering the temperature constant inside the zone, and consequently, the reactivity variation. In this way, the calculation of the integral between eigenfunction and its adjoint over the zone can be performed once during the offline process, and it is kept constant during the transient simulation. Indeed, this quantity is multiplied by the removal (or production) variation, which is temperature and density dependent (and, therefore, also time dependent). According to this procedure, $\underline{\underline{\delta L}}_{im}$ can be expressed as follows

$$
\begin{aligned}
\underline{\underline{\delta L}}_{im}(d,T) &= \int \underline{\underline{\psi}}_i^{\dagger} \cdot \delta L(d,T) \underline{\underline{\psi}}_m \, \mathrm{d}\Omega \\
&= \sum_{gz} \int \underline{\underline{\psi}}_i^{\dagger} \cdot \Big[-\nabla \cdot (\underline{\underline{D}}(d_{gz},T_{gz})\nabla) \\
&\quad + \underline{\underline{\Sigma}}_a(d_{gz},T_{gz}) + \underline{\underline{\Sigma}}_s(d_{gz},T_{gz}) \Big] \underline{\underline{\psi}}_m \, \mathrm{d}\Omega_{gz} \\
&= \sum_{gz} \Bigg[\int \nabla \underline{\underline{\psi}}_i^{\dagger} \cdot \underline{\underline{D}}(d_{gz},T_{gz}) \nabla \underline{\underline{\psi}}_m \, \mathrm{d}\Omega_{gz} \\
&\quad - \int_{\partial\Omega_{gz}} \underline{\underline{\psi}}_i^{\dagger} \cdot (\boldsymbol{n} \cdot \underline{\underline{D}}(d_{gz},T_{gz}) \nabla \underline{\underline{\psi}}_m) \mathrm{d}S_{gz} \\
&\quad + \int \underline{\underline{\psi}}_i^{\dagger} \cdot \underline{\underline{\Sigma}}_a(d_{gz},T_{gz}) \cdot \underline{\underline{\psi}}_m \, \mathrm{d}\Omega_{gz} \\
&\quad + \int \underline{\underline{\psi}}_i^{\dagger} \cdot \underline{\underline{\Sigma}}_s(d_{gz},T_{gz}) \cdot \underline{\underline{\psi}}_m \, \mathrm{d}\Omega_{gz} \Bigg] \\
&= \sum_{gz} \Bigg[\underline{\underline{D}}(d_{gz},T_{gz}) \int \nabla \underline{\underline{\psi}}_i^{\dagger} \cdot \nabla \underline{\underline{\psi}}_m \, \mathrm{d}\Omega_{gz} \\
&\quad + \underline{\underline{\Sigma}}_a(d_{gz},T_{gz}) \int \underline{\underline{\psi}}_i^{\dagger} \cdot \underline{\underline{\psi}}_m \, \mathrm{d}\Omega_{gz} \\
&\quad + \underline{\underline{\Sigma}}_s(d_{gz},T_{gz}) \int \underline{\underline{\psi}}_i^{\dagger} \cdot \underline{\underline{\psi}}_m \, \mathrm{d}\Omega_{gz} \Bigg] \\
&\quad + \gamma_r \int_{\partial\Omega_r} \underline{\underline{\psi}}_i^{\dagger} \cdot \underline{\underline{\psi}}_m \, \mathrm{d}S_r + \gamma_a \int_{\partial\Omega_a} \underline{\underline{\psi}}_i^{\dagger} \cdot \underline{\underline{\psi}}_m \, \mathrm{d}S_a
\end{aligned} \tag{19}
$$

where the Green's first identity has been applied to the diffusion operator and, in the final form, the corresponding surface integrals can be computed only on the radial $\partial\Omega_r$ and axial boundary $\partial\Omega_a$ of the domain. Moreover, the summation is carried out over the zones in which the domain has been divided.

In a control-oriented perspective, it is fundamental that the model provides three integral quantities of interest, i.e., the neutron flux, the fission power, and the reactivity (the white output triangles in Fig. 3). These quantities are not directly available from Eqs. (16) and (17), and additional calculations are needed. As far as the power is concerned, it is provided to the *FuelPin_Lead* through a connector in order to calculate the temperature distribution inside the fuel pin.

The neutron flux can be evaluated through the integrals of the eigenfunctions suitably normalized. Indeed, the eigenfunction does not report any information about the actual value, the neutron flux being normalized during the offline computation. The information can be retrieved by calculating a reference flux ϕ^{ref}, i.e., referred to the unperturbed initial condition. In this way, the neutron flux reads as

$$
\underline{\phi}(t) = K\phi^{\mathrm{ref}} \sum_{j=1}^{N} \left[\left(\int \underline{\underline{\psi}}_j \, \mathrm{d}\Omega \right) \cdot \underline{n}_j(t) \right] \tag{20}
$$

where the constant K is computed with respect to the initial condition $\Phi(0) = \phi^{\mathrm{ref}}$.

As far as the fission power is concerned, this value can be retrieved from the neutron flux in the fuel zone, previously calculated for the reactivity feedback assessment

$$
q(t) = K\phi^{\mathrm{ref}} V \sum_{z=\mathrm{fuel}} \sum_{j=1}^{N} \left[\left(\int E_f \underline{\underline{\Sigma}}_f \cdot \underline{\underline{\psi}}_j \, \mathrm{d}\Omega z \right) \cdot \underline{n}_j(t) \right] \tag{21}
$$

Finally, the reactivity can be monitored both to assess the capabilities of the MM compared with other approaches and to monitor this relevant quantity during the simulated transients. The system reactivity can be estimated via the inverse method [18]. Nevertheless, this method is not particularly suitable in case of sharp time-dependent variation of the reactivity as it exploits the concept of the "stable period." A formulation similar to the reactivity assessment in transport theory can be proposed [19], exploiting the choice of the adjoint eigenfunctions as test functions

$$
\rho(t) = \frac{\int \mathrm{d}\Omega \phi^{\dagger} [\mathcal{L}\phi + [(1-\beta)\chi_p + \beta\chi_d]\mathcal{F}\phi]}{\int \mathrm{d}\Omega \phi^{\dagger} [[(1-\beta)\chi_p + \beta\chi_d]\mathcal{F}\phi]} \tag{22}
$$

According to the MM, Eq. (22) can be formulated as follows

$$
\begin{aligned}
\rho(t) &= \frac{\underline{n}^T \cdot [\underline{\underline{A}}_{1,np} + \underline{\underline{A}}_{1,p} + \beta \underline{\underline{A}}_{md}] \cdot \underline{n}}{\underline{n}^T \cdot [(1-\beta)\underline{\underline{A}}_{mp} + \beta \underline{\underline{A}}_{md}] \cdot \underline{n}} \\
\underline{\underline{A}}_{md} &= \begin{bmatrix} \underline{X} \cdot (\underline{\underline{M}}_{11} + \underline{\underline{\delta M}}_{11}) & \cdots & \underline{X} \cdot (\underline{\underline{M}}_{1N} + \underline{\underline{\delta M}}_{1N}) \\ \vdots & \ddots & \vdots \\ \underline{X} \cdot (\underline{\underline{M}}_{N1} + \underline{\underline{\delta M}}_{N1}) & \cdots & \underline{X} \cdot (\underline{\underline{M}}_{NN} + \underline{\underline{\delta M}}_{NN}) \end{bmatrix} \\
\underline{\underline{A}}_{mp} &= \begin{bmatrix} \underline{\underline{M}}_{11} + \underline{\underline{\delta M}}_{11} & \cdots & \underline{\underline{M}}_{1N} + \underline{\underline{\delta M}}_{1N} \\ \vdots & \ddots & \vdots \\ \underline{\underline{M}}_{N1} + \underline{\underline{\delta M}}_{N1} & \cdots & \underline{\underline{M}}_{NN} + \underline{\underline{\delta M}}_{NN} \end{bmatrix}
\end{aligned} \tag{23}
$$

3.2 FuelPin_Lead Component. The *FuelPin_Lead* component, divided into the *FuelPinHT* and *LeadTube* subcomponents, is devoted to the evaluation of the dynamic behavior of the fuel pin and lead temperatures. The modeling of the heat transfer is of paramount importance as the temperature field appears in the reactivity assessment (see Eq. (19)). The *FuelPinHT* component is dedicated to the heat transfer in the fuel rods, adopting radial regions within the element. This component has been developed ad hoc in order to obtain some advisable features (i.e., modularity, reusability, and efficiency) in an object-oriented perspective. As far as the *LeadTube* is concerned, a standard component of the *ThermoPower* library modeling the coolant flowing through the core channels (represented as cylindrical conduits) has been adopted. Hereinafter, the attention is focused on the *FuelPinHT* modeling, whereas for the *LeadTube* component, the reader can refer to Refs. [9,25].

3.2.1 FuelPinHT Component. As far as the *FuelPinHT* modeling is concerned, the time-dependent Fourier equation (Eq. (24)) has been applied considering only the radial heat transfer, thus disregarding both the axial and the circumferential thermal diffusion. The equation has been discretized radially in different cylindrical zones and longitudinally in a user-defined number of nodes (Fig. 4).

$$
dc_p \frac{\partial T}{\partial t} = \nabla \cdot (k \nabla T) + Q''' \tag{24}
$$

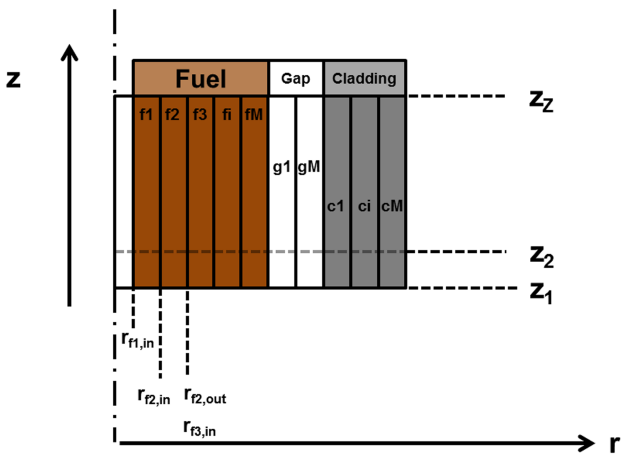

Fig. 4 Axial and radial discretization of the fuel pin

The common discretization procedure [26] is to integrate twice, first performing an indefinite integration and then integrating from r_{in} to r_{out} and T_{in} to T_{out}, which are the inner and the outer radius and temperature of the considered cylindrical zone, respectively. After the first integration, the equation reads

$$dc_p \frac{\mathrm{d}T}{\mathrm{d}t}\frac{r}{2} = k\frac{\mathrm{d}T}{\mathrm{d}r} + Q'''\frac{r}{2} + \frac{C}{r} \tag{25}$$

where C represents the constant of the indefinite integration. In order to set a value for the constant, a boundary condition is applied on the heat flux at r_{in} or r_{out}. In particular, for the inner zone, the vanishing of the flux at r_{in} is set

$$q''_{f1}|_{r=r_{f1,in}} = -k\left.\frac{dT_{f1}}{dr}\right|_{r=r_{f1,in}} = 0 \tag{26}$$

On the other hand, for the other zones, the continuity of the heat flux between adjacent zones is used for determining the constant. For example, between two generic adjacent zones, $f2$ and $f3$, it reads

$$q''_{f2}|_{r=r_{f2,out}} = q''_{f3}|_{r=r_{f3,in}} \rightarrow -k\left.\frac{\mathrm{d}T_{f2}}{\mathrm{d}r}\right|_{r=r_{f2,in}} = -k\left.\frac{\mathrm{d}T_{f3}}{\mathrm{d}r}\right|_{r=r_{f3,out}} \tag{27}$$

Usually, in the determination of the constant C, the term in Eq. (25) involving the time derivative is neglected as this procedure is normally applied for stationary calculation. Notwithstanding, as far as dynamics simulation is concerned, the time-dependent behavior is relevant and this aspect cannot be left apart. For example, for the inner zone $f1$, the constant C reads

$$C_{f1} = -Q'''\frac{r^2_{f1,in}}{2} + dc_p\frac{\mathrm{d}T}{\mathrm{d}t}\frac{r^2_{f1,in}}{2} \tag{28}$$

where the second term from the right allows for the transient behavior of the temperature. For the other zones, it is possible to express the constant in a recursive way, starting from the C of the inner adjacent zone

$$C_{f3} = C_{f2} + \left[(Q'''_{f2} - Q'''_{f3}) - \left(d_{f2}c_{p,f2}\frac{\mathrm{d}T_{f2}}{\mathrm{d}t} - d_{f3}c_{p,f3}\frac{\mathrm{d}T_{f3}}{\mathrm{d}t}\right)\right]\cdot\frac{r^2_{f3,in}}{2} \tag{29}$$

The heat equation, after the final integration, reads

$$dc_p\frac{\mathrm{d}T}{\mathrm{d}t}\frac{r^2_{out}-r^2_{in}}{4} = k(T_{out}-T_{in}) + Q'''\frac{r^2_{out}-r^2_{in}}{4} + C\cdot\log\left(\frac{r_{out}}{r_{in}}\right) \tag{30}$$

As a closure equation for the temperature T, a volume-averaged expression has been adopted

$$T = T_{in} - \frac{r^2_{out}-r^2_{in}}{8k}\left(Q''' + dc_p\frac{\mathrm{d}T}{\mathrm{d}t}\right) - \frac{C}{k}\left(\frac{r^2_{out}}{r^2_{out}-r^2_{in}}\log\left(\frac{r_{out}}{r_{in}}\right) - \frac{1}{2}\right) \tag{31}$$

The presented procedure ensures an extremely high degree of flexibility as the user can select the number of the radial and axial zones of the fuel pin discretization, optimizing the balance between model accuracy and time simulation cost. For the present case, in order to be coherent with the neutronics modeling, three zones for the fuel have been selected, one for the gap and others for cladding. For each radial zone, Eq. (30) is implemented and discretized in Z nodes, specifying the material properties [27] and whether it is a fuel zone or not. In particular, if it is a fuel zone, the power Q''' is provided from the MN component through a connector (Fig. 3). Once established with the number and the type of the zones, the modeling is completed specifying the integration constant in a recursive way (see Eqs. (28) and (29)).

4 Simulation Results

The capabilities of the proposed object-oriented tool have been evaluated in two different kinds of simulation. The first is devoted to the reactivity evaluation in order to assess how the MN component can predict the reactivity variation. The model performance has been evaluated against the reference model (i.e., the multigroup diffusion equations) and the classic PK. The second type of simulation concerns the dynamic behavior of the system. In particular, the object-oriented model has been compared to the reference model during some typical transients, i.e., an enhancement of the lead inlet temperature and an externally imposed reactivity insertion.

4.1 Reactivity Comparison. One of the main requirements of a control-oriented simulator is to accurately evaluate the reactivity variation following a temperature change. Accordingly, the capability of the MN component to correctly reproduce this trend has been assessed in several cases imposing an arbitrary temperature variation and reporting the reactivity insertion (or extraction) due to the resulting cross-section variation (see Eq. (19)). As the main purpose is to assess only the reactivity change, the *FuelPin_Lead* has not taken into account, considering the temperature variation as an input for the MN component.

Regarding the reference model, the reactivity variation has been evaluated as difference of the first eigenvalues between the unperturbed case and the perturbed one. As far as the MN component is concerned, the reactivity has been evaluated according to Eq. (23). Eventually, the reactivity value related to the PK has been assessed in a classic way

$$\rho_{PK} = \alpha_f\cdot(\bar{T}_f - \bar{T}_{f,0}) + \alpha_l\cdot(\bar{T}_l - \bar{T}_{l,0}) \tag{32}$$

The fuel and lead reactivity coefficients of Eq. (32) have been obtained from the SERPENT calculation, and the fuel and lead temperatures have been evaluated as weighted average of the temperature profiles of the fuel and lead. Three different temperature profiles have been studied as test cases in order to underline the PK limits and the MM potentiality

1. Uniform temperature decrease, $\Delta T_{f1} = -50$ K, $\Delta T_{f2} = -50$ K, $\Delta T_{f3} = -50$ K, $\Delta T_l = -50$ K
2. Temperature enhancement in a single pin and in the fifth axial slice, i.e., $\Delta T_{f1} = +400$ K, $\Delta T_{f2} = +300$ K, $\Delta T_{f3} = +200$ K, $\Delta T_l = +100$ K
3. Shutdown scenario: all the temperatures are set equal to the inlet lead temperature (i.e., $T = 673.15$ K)

In Table 3, the reactivity inserted in the system for each case and for the three neutronics modeling approaches (i.e., PK, MN component, and the multigroup diffusion PDEs) are shown. For the

Table 3 Reactivity comparison results for the three cases studied

	Reactivity inserted (pcm)		
Neutronics modeling approach	Case 1	Case 2	Case 3
Multigroup diffusion PDEs (reference)	78.4	−25.5	1267.6
Modal neutronics component (MN)	78.8	−25.6	1268.9
Point kinetics (PK)	81	−18.9	1363.8

Table 4 Computational time of the object-oriented model compared with the reference model

Neutronics modeling approach	Computational time			
Multigroup diffusion PDEs (reference)	40 h			
Object-oriented model	$N = 1$	$N = 3$	$N = 5$	$N = 10$
	10 s	23 s	45 s	143 s

MN component, seven eigenfunctions have been employed as spatial basis.

The results show a very good agreement between the value obtained from the reference model and the MN component, assessing the desired capabilities of the proposed model. On the other hand, especially in test cases 2 and 3, the reactivity assessed by the PK differs greatly from the other values. In particular, case 1 shows that the PK is able to properly predict the reactivity inserted in the system whether the perturbation (i.e., the temperature variation) is uniform. Nevertheless, the temperature evolution in operational transient is not uniform. Case 2, representing the extreme opposite case of a strong localized perturbation, is useful to assess the MN capabilities and the PK limit. Case 3 is relevant because it represents an operational situation, i.e., all the temperatures are set at 400°C as in shutdown condition. In this case, the perturbation is neither localized nor uniform. The PK overestimates the reactivity insertion of almost 8%, whereas the MN value has a very good agreement with the reference one.

4.2 Transient Comparison. Another requirement demanded for a control-oriented simulator is the capability to reproduce the transient behavior of the main variables of interest (first, the power but also the system temperatures and reactivity). For this purpose, in the object-oriented model, the MN component has been linked with the *FuelPin_Lead* component so as to provide the dynamic model for the temperature evolution. Two typical transient scenarios have been simulated, namely, a 20°C enhancement of the inlet lead temperature and a 100-pcm reactivity insertion. The simulation outcomes of the object-oriented model have been compared to the reference time-dependent solution of the multigroup diffusion PDEs ((Eqs. (1) and (2)). As mentioned in Section 1, the computational time of the object-oriented model should fulfill the fast-running request for control-oriented purposes. In Table 4, the computational times[2] of the object-oriented model and the reference one for the simulation concerning the enhancement of the inlet lead temperature (simulated time of 50 s) are provided.

The following simulations have been obtained with five eigenfunctions, achieving a good compromise between accuracy and computational cost.

4.2.1 Enhancement of the Inlet Lead Temperature. The simulation has been performed by increasing the inlet lead temperature by 20°C. The system response is well represented by the total pin power shown in Fig. 5, where the outcomes of the object-oriented model (solid line) and the reference model developed in COMSOL (dashed line) are presented. The satisfactory agreement confirms the capabilities of the developed tool also in transient simulation. Due to the increase in the lead temperature entering the channel (Fig. 6), a positive reactivity is inserted in the system (Fig. 7). After 1–2 s, the negative reactivity insertion, mainly due to the Doppler effect caused by the increase of the fuel temperature, sets the power to a lower level (Fig. 5).

4.2.2 Reactivity Insertion. A reactivity insertion of 100 pcm has been simulated. As in the previous case, the figure of merit for the comparison between the object-oriented model (dashed line) and the reference model (solid line) is the pin power (Fig. 8).

[2]The object-oriented model has been run with a laptop (2.20 GHz, 8 GB RAM). The multigroup diffusion PDEs have been solved with a workstation (8 × 2.8 GHz, 64 GB RAM).

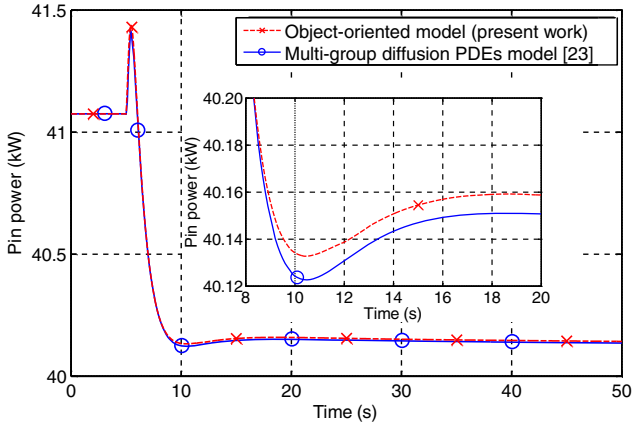

Fig. 5 Pin power variation following a lead inlet temperature enhancement

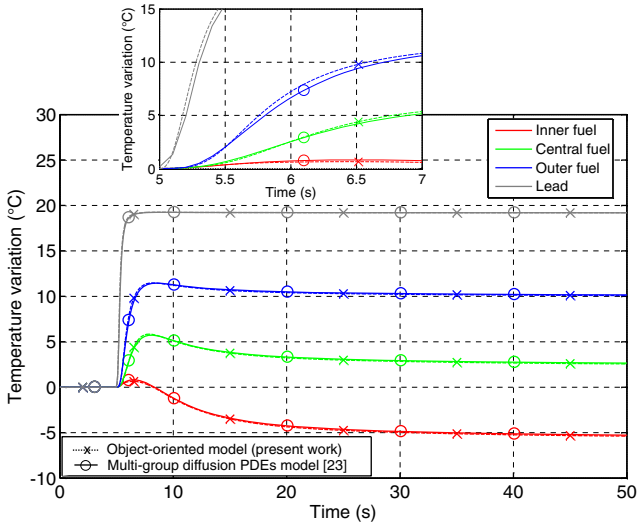

Fig. 6 Fuel and lead temperature variations following a lead inlet temperature enhancement

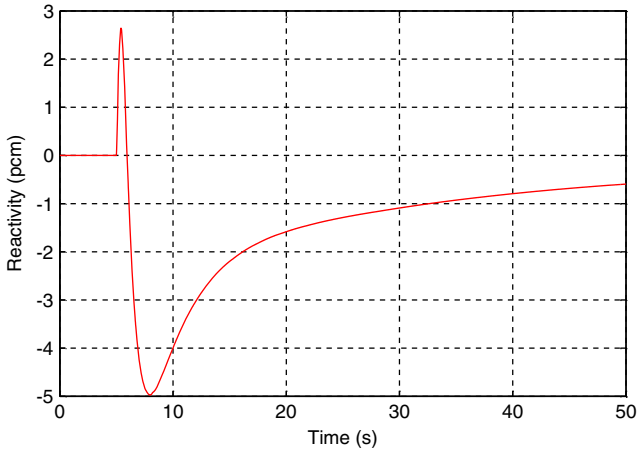

Fig. 7 Reactivity variation following a lead inlet temperature enhancement

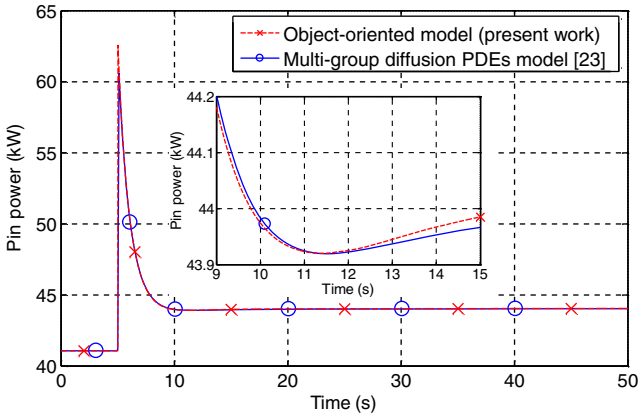

Fig. 8 Pin power variation following a reactivity insertion

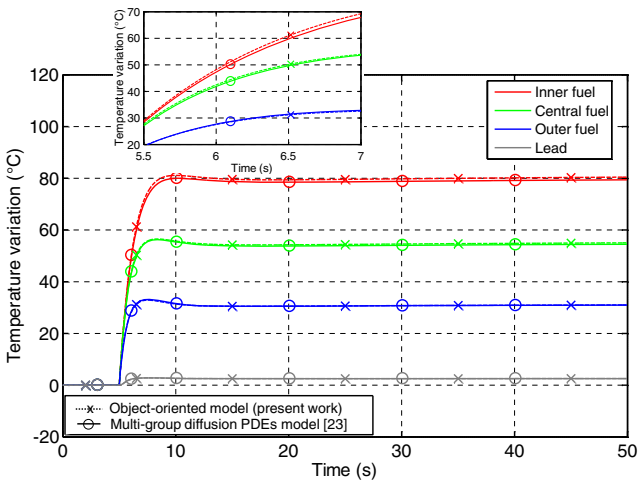

Fig. 9 Fuel and lead temperature variation following a reactivity insertion

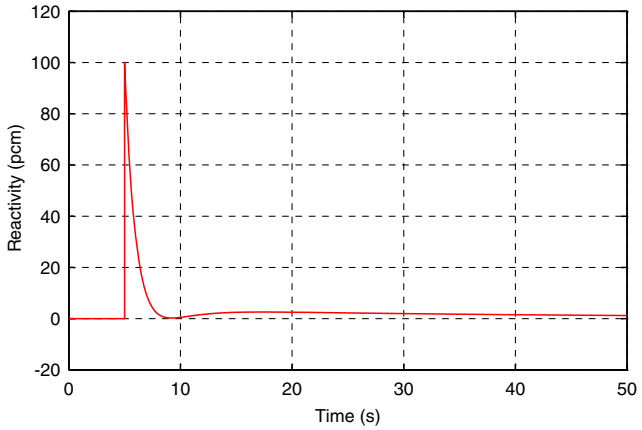

Fig. 10 Reactivity variation following a reactivity insertion

A good agreement between the object-oriented model and the reference model also for this simulation has been achieved. After the prompt power increase, the corresponding enhancement of the fuel temperature (Fig. 9) introduces a negative reactivity, limiting the power and restoring the criticality (Fig. 10).

5 Conclusions

This work presents an object-oriented simulation tool for control purposes. It implements both a spatial neutronics component based on the MM and a fuel pin heat-transfer component. The MN component has been developed starting from the neutron diffusion equation whose eigenfunctions have been exploited to separate the spatial and time dependence of the neutron flux. Once the eigenfunctions and related integrals have been calculated, the MM leads to a set of ODEs, which can be used to study the system dynamics in typical transients of interest for control purposes with a reduced computational burden. In this paper, a case study involving three fuel pins of an innovative LFR has been set up and investigated, even if the proposed method and modeling approach can be applied to any reactor concept.

The adopted description allows for the spatial heterogeneity of the system, in particular, as far as the thermal reactivity feedbacks are concerned, providing a spatial representation of the neutron flux. In this perspective, the adoption of a proper object-oriented component devoted to the heat transfer of both the fuel pin and the lead turns out to be useful for exploiting the features of this modeling approach.

The developed object-oriented simulation tool constitutes a considerable step forward compared to the neutronics models that are currently used in the control-oriented tools (i.e., compared to a PK approach). As a major outcome of the simulation results, the object-oriented model based on the MN component proved suitable to represent both the static reactivity variation and the dynamics behavior of the system. In particular, the results have been compared with a reference model based on the solution of the multi-group diffusion PDEs, outlining a good agreement between the two approaches.

In short, this work is meant to be a preliminary investigation on the feasibility of the proposed MN component to study the reactor dynamics and to be employed in control-oriented simulations, being accurate in both the reactivity and transient representation without an excessive computational cost. The modeling of the entire core at fuel assembly level is envisaged in future works as well as the study of other techniques (e.g., see [15]) to be employed in the neutronics characterization of control-oriented tools.

Nomenclature

Latin Symbols

A = coefficient used in Eq. (9), cm^{-1}
C_j = concentration of the jth precursor group, cm^{-3}
c = generic cladding zone
c_p = heat capacity, $\mathrm{J\,kg^{-1}\,K^{-1}}$
D_g = neutron diffusion coefficient of the gth energy group, cm
d = density, $\mathrm{g\,cm^{-3}}$
E = energy, MeV
E_f = average energy released per fission event, J
$\mathcal{F}$ = fission operator of transport theory
f = generic fuel zone
g = generic gap zone
$\underline{\underline{I}}$ = identity matrix of 6×6 size, –
$\underline{\underline{k}}$ = thermal conductivity, $\mathrm{W\,cm^{-1}\,K^{-1}}$
$\mathcal{L}$ = removal operator of transport theory
M = number of radial nodes, –
N = number of employed eigenfunctions, –
$\boldsymbol{n}$ = surface normal unit vector, –
n_i^g = time-dependent coefficient of the ith spatial eigenfunction of the neutron flux of the gth energy group, –
P = number of precursor groups employed, –
Q''' = volumetric heat source, $\mathrm{W\,cm^{-3}}$
q = power, W
q'' = heat flux, $\mathrm{W\,cm^{-2}}$
r = radius, cm
r_{in} = inner radius of generic cylindrical zone

r_{out} = outer radius of generic cylindrical zone
$\boldsymbol{r}$ = spatial coordinate, cm
S = surface of the spatial domain, cm^2
T = temperature, K
$\bar{T}$ = mean temperature, K
t = time, s
V = fuel volume, cm^3
v_g = neutron speed of the g-th energy group, $cm\,s^{-1}$
Z = number of axial nodes, –
z = axial coordinate
$\underline{\underline{0}}$ = zero matrix of 6×6 size, –

Greek Symbols

α = reactivity coefficient used in Eq. (32), $pcm\,K^{-1}$
β = total delayed neutron fraction, pcm
β_j = delayed neutron fraction of the jth precursor group, pcm
γ = albedo coefficient used in Eq. (11), –
λ_j = decay constant of the jth precursor group, s^{-1}
λ_i^* = ith eigenvalue, –
ν = average number of neutrons emitted per fission event, –
ρ = reactivity, pcm
Σ = generic macroscopic cross section, cm^{-1}
Σ_a^g = macroscopic absorption cross section of the gth energy group, cm^{-1}
Σ_f^g = macroscopic fission cross section of the gth energy group, cm^{-1}
$\Sigma_s^{g\rightarrow}$ = macroscopic cross section including scattering out of the energy group g, cm^{-1}
$\Sigma_s^{g\rightarrow g'}$ = macroscopic group transfer cross section from energy group g to g', cm^{-1}
ϕ_g = neutron flux of the gth energy group, $cm^{-2}\,s^{-1}$
χ_d^g = fraction of delayed neutrons generated in the gth energy group, –
χ_p^g = fraction of prompt neutrons generated in the gth energy group, –
ψ_i^g = ith spatial eigenfunction of the neutron flux of the gth energy group, $cm^{-2}\,s^{-1}$
$\psi_i^{\dagger g}$ = ith spatial eigenfunction of the adjoint neutron flux of the gth energy group, –
Ω = spatial domain, cm^3

Subscripts

0 = reference value
a = axial
f = fuel
$f1$ = inner fuel zone
$f2$ = central fuel zone
$f3$ = outer fuel zone
g = energy group number
gz = generic zone
in = inner
l = lead
out = outer
PK = point kinetics
r = radial

References

[1] IAEA, 1999, "Modern Instrumentation and Control for Nuclear Power Plants: A Guidebook," *Technical Reports Series No. 387*, International Atomic Energy Agency, Vienna.

[2] IAEA, 2009, "Implementing Digital Instrumentation and Control Systems in the Modernization of Nuclear Power Plants," *IAEA Nuclear Energy Series NP-T-1.4*, International Atomic Energy Agency, Vienna.

[3] GIF, 2002, "A Technology Roadmap for Generation IV Nuclear Energy System," US DOE Nuclear Energy Research Advisory Committee and the Generation IV International Forum, *Technical Report, Report No. GIF-002-00*.

[4] Fritzson, P., 2004, *Principles of Object-Oriented Modeling and Simulation with Modelica 2.1*, Wiley-IEEE Press, New York, NY.

[5] Modelica, 2011, http://www.modelica.org.

[6] Fritzson, P., 2011, "A Cyber-Physical Modeling Language and the OpenModelica Environment," Proceedings of the International Wireless Communications and Mobile Computing Conference, Turkey, July 4–8, IEEE, Piscataway, NJ, pp. 1648–1653.

[7] Cammi, A., Casella, F., Ricotti, M. E., and Schiavo, F., 2005, "Object-Oriented Modelling, Simulation and Control of IRIS Nuclear Power Plant with Modelica," Proceedings of the 4th International Modelica Conference, Hamburg, Germany, Mar. 7–8, The Modelica Association and the Department of Thermodynamics, Hamburg University of Technology, Hamburg, Germany, pp. 423–432.

[8] Souyri, A., Bouskela, D., Pentori, B., and Kerkar, N., 2006, "Pressurized Water Reactor Modelling with Modelica," Proceedings of the 5th International Modelica Conference, Vienna, Austria, Sept. 4–5, The Modelica Association and the Arsenal Research, Vienna, Austria, pp. 127–133.

[9] Ponciroli, R., Bigoni, A., Cammi, A., Lorenzi, S., and Luzzi, L., 2014, "Object-Oriented Modelling and Simulation for the ALFRED Dynamics," Prog. Nucl. Energy, **71**, pp. 15–29.

[10] Schultz, M. A., 1961, *Control of Nuclear Reactors and Power Plants*, McGraw-Hill, New York.

[11] Hetrick, D. L., 1993, *Dynamics of Nuclear Reactors*, American Nuclear Society, Inc., La Grange Park, IL.

[12] Stacey, W. M., 1969, *Space-Time Nuclear Reactor Kinetics*, Academic Press, Waltham, MA.

[13] Dulla, S., Picca, P., and Ravetto, P., 2009, "Variational Methods in the Kinetic Modeling of Nuclear Reactors: Recent Advances," Proceedings of the International Conference on Mathematics, Computational Methods and Reactor Physics, Saratoga Springs, NY, May 3–7, American Nuclear Society, LaGrange Park, IL.

[14] Xia, L., Jiang, J., Javidnia, H., and Luxat, J. C., 2012, "Performance Evaluation of a 3-D Kinetic Model for CANDU Reactors in a Closed-Loop Environment," Nucl. Eng. Des., **243**, pp. 76–86.

[15] Sartori, A., Baroli, D., Cammi, A., Chiesa, D., Luzzi, L., Ponciroli, R., Previtali, E., Ricotti, M. E., Rozza, G., and Sisti, M., 2013, "Comparison of a Modal Method and a Proper Orthogonal Decomposition Approach for Multi-Group Time-Dependent Reactor Spatial Kinetics," Ann. Nucl. Energy, **71**, pp. 217–229.

[16] Alemberti, A., Frogheri, M., and Mansani, L., 2013, "The Lead Fast Reactor Demonstrator (ALFRED) and ELFR Design," Proceedings of the IAEA International Conference on Fast Reactors and Related Fuel Cycles: Safe Technologies and Sustainable Scenarios, Paris, France, Mar. 4–7, International Atomic Energy Agency, Vienna, Austria, Paper No. IAEA-CN-199/437.

[17] Grasso, G., Petrovich, C., Mattioli, D., Artioli, C., Sciora, P., Gugiu, D., Bandini, G., Bubelis, E., and Mikityuk, K., 2014, "The Core Design of ALFRED, a Demonstrator for the European Lead-Cooled Reactors," Nucl. Eng. Des., **278**, pp. 287–301.

[18] Duderstadt, J. J., and Hamilton, L. J., 1976, *Nuclear Reactor Analysis*, John Wiley and Sons, New York.

[19] Henry, A. F., 1975, *Nuclear Reactor Analysis*, The MIT Press, Cambridge, MA.

[20] COMSOL, 2011, "COMSOL Multiphysics® 4.2a, User's Guide," COMSOL Inc., Stockholm, Sweden.

[21] SERPENT, 2011, "PSG2/Serpent Monte Carlo Reactor Physics Burnup Calculation Code," http://montecarlo.vtt.fi.

[22] Aufiero, M., Cammi, A., Fiorina, C., Luzzi, L., and Sartori, A., 2013, "A Multiphysics Time-Dependent Model for the Lead Fast Reactor Single-Channel Analysis," Nucl. Eng. Des., **256**, pp. 14–27.

[23] Lorenzi, S., Cammi, A., Luzzi, L., and Ponciroli P., 2014, "Development of a Spatial Neutronics Model for Control-Oriented Dynamics Simulation," Proceedings of the International Conference On Nuclear Engineering, Prague, Czech Republic, July 7–11, Paper No. 30818.

[24] Elmqvist, H., Cellier, F. E., and Otter, M., 1993, "Object-Oriented Modeling of Hybrid Systems," Proceedings of the European Simulation Symposium (ESS'93), Delft, Netherlands, Oct. 25–28, SCS Publisher, La Jolla, CA, pp. 31–41.

[25] Casella, F., and Leva, A., 2006, "Modeling of Thermo-Hydraulic Power Generation Processes Using Modelica," Math. Comput. Model. Dyn. Sys., **12**(1), pp. 19–33.

[26] Todreas, N. E, and Kazimi, M. S., 2012, Nuclear Systems, *Thermal Hydraulic Fundamentals*, Vol. **1**, Taylor & Francis, Boca Raton, FL.

[27] Luzzi, L., Cammi, A., Di Marcello, V., Lorenzi, S., Pizzocri, D., and Van Uffelen, P., 2014, "Application of the TRANSURANUS Code for the Fuel Pin Design Process of the ALFRED Reactor," Nucl. Eng. Des., **277**, pp. 173–187.